A classical ensemble model of three-body collisions in the point contact approximation and application to alignment effects in near-resonant energy transfer collisions of He atoms with Rydberg Ca atoms

Neil E. Shafer-Ray, Michael A. Morrison,[a] and Gregory A. Parker
Department of Physics and Astronomy, University of Oklahoma, Norman, Oklahoma 73019-0225

(Received 29 November 1999; accepted 31 May 2000)

A classical ensemble model of three-body energy transfer in the point contact approximation is presented. This model yields cross sections for transitions between initial and final states defined by energy, magnitude of angular momentum, and projection of angular momentum along an axis of spatial quantization corresponding to the quantum numbers of the initial and final stationary states, n,l,m and n',l',m'. Using a cross section that is differential in the final-state quantum numbers, the spatial constraints imposed by conservation of energy and angular momentum can be investigated even for comparatively small quantum numbers. When applied to the $\mathrm{Ca}(17d)+\mathrm{He}\rightarrow\mathrm{Ca}(18p)+\mathrm{He}$ energy transfer processes, the model sheds light on recently discovered alignment phenomena in collisions of rare-gas atoms with initially aligned Rydberg atoms. Materials for the implementation of this model are available from the authors via the Internet. © *2000 American Institute of Physics.* [S0021-9606(00)03032-4]

I. INTRODUCTION

In this paper we present a classical transport model of energy transfer in heavy-particle collisions within the Fermi point contact approximation.[1] Although fully classical, this model incorporates quantization of energy and angular momenta in both the initial and final states. As a first application of this model, we consider near-resonant energy transfer collisions involving initially aligned Rydberg Ca atoms and a rare-gas perturber: specifically, the scattering process

$$\mathrm{Ca}(4s17d\ ^1D_2)+\mathrm{He}\rightarrow\mathrm{Ca}(4s18p\ ^1P_1)+\mathrm{He}. \tag{1}$$

Recent experimental and theoretical studies of such collisions[2,3] have raised provocative qualitative questions which the present classical model can address. No classical model can, of course, produce quantitatively accurate cross sections for such a system. Our classical cross sections are, however, in sufficient qualitative agreement with quantum-mechanical results that we consider their implications relevant for the actual scattering process. Moreover, this model can yield insights that would be difficult to glean from full quantum-mechanical investigations. For example, for the Ca–He collision (1), we have determined the transition probability as a correlated function of the relative velocity of the rare-gas projectile and the distance of the Rydberg electron from the Ca^+ core at the time of the collision. This probability clarifies whether the interaction occurs far from the core, where the Coulomb wave function describes the electron, or near the core, where the core can significantly influence the electron.

In the laboratory, processes such as (1) are studied by first aligning the initial state of the Rydberg electron (e.g., via multiple pulsed-laser excitation), then analyzing measured inelastic cross sections for effects such as a dependence on the angle between the polarization of the exciting laser and the relative velocity of the rare-gas projectile.[4–7] If present, such effects signal that the excited electron ''remembers'' its initial alignment through the collision.[8,7] Until recently, all investigations of alignment in near-resonant energy transfer collisions have considered targets in *low-lying* excited states, not Rydberg states.[7] For such targets, the qualitative explanation of alignment effects has been predicated on the formation during the collision of a transient quasimolecular electronic state. According to these ''orbital following'' and ''locking'' models,[5,9,10] the orbital of the excited electron temporarily couples to the internuclear axis of the quasimolecule. Consequently, depending on the distance at which the orbital locks and on the symmetry of the resulting electronic state, cross sections may exhibit alignment effects of varying degree. Such models, however, are not germane to collisions with *Rydberg* atoms, where the electron's comparatively low speed and extremely diffuse probability density invalidate a molecular (Born–Oppenheimer) description of the dynamics.[11,12] Hence, cross sections for rare-gas collisions with *Rydberg* atoms were not expected to manifest alignment effects.

Nevertheless, measurements by Spain *et al.*[13,14] revealed unambiguous alignment effects in cross sections for the $17d\rightarrow18p$ transition in Ca resulting from collisions with ground-state Xe atoms at a single mean relative velocity. Quantum calculations by Isaacs and Morrison[15,2] confirmed these results and, by exploring a wide range of relative velocities, uncovered heretofore unknown oscillatory structures in the cross sections for this transition. These authors also investigated analogous scattering processes for Ca–He collisions, finding qualitatively identical phenomena in state-to-state cross sections. These findings raised questions concerning the origin of the alignment effects, the physical

[a]Electronic mail: morrison@mail.nhn.ou.edu

mechanism responsible for the oscillations, and reason for their striking dependence on the initial and final magnetic quantum numbers of the Rydberg electron.

A coterminious semiclassical time-dependent analysis of the Ca–He system by Morrison *et al.*[3] revealed the physical mechanism behind the oscillations in the state-to-state energy transfer cross sections[3] but left unexplained the alignment effects themselves. Alignment effects most clearly manifest in partial magnetic sublevel cross sections $\sigma^{|m|}(v)$. To construct these, one first calculates state-to-state cross sections as a function of the relative Ca–He velocity u_r for the transitions $\alpha=(n,l,m)\rightarrow\alpha'=(n',l',m')$ for all magnetic quantum numbers m and m' allowed by the orbital angular momentum quantum numbers l and l' of the excitation $(n,l)\rightarrow(n',l')$. One then sums the resulting cross sections over final state m' for each initial m. *The extent to which each of the resulting partial cross sections* $\sigma^{|m|}(v)$ *depends on* $|m|$ *at a particular relative velocity* v *is a measure of the strength of the alignment effect: if these quantities are independent of* $|m|$*, then no such effects are present and the collision has obliterated all information concerning the initial alignment of the Rydberg electron.*[7] Figure 1 shows pronounced oscillatory alignment effects in partial magnetic cross sections for the $17d\rightarrow18p$ transition in Ca–He collisions. This figure also illustrates the striking concurrence of cross sections from the aforementioned quantum-mechanical and semiclassical studies. The present classical model completes our theoretical triumvirate of studies of this problem and provides insight into the underlying physics behind the alignment effects in scattering process such as the one in Fig. 1.

More generally, our model provides an efficient method for calculating energy transfer cross sections of sufficient accuracy to provide estimates of quantities needed for experimental design. In addition, it offers a possible avenue for investigating the appearance in semiclassical or approximate quantal calculations of false resonances—spurious peaks in the energy dependence of the cross section for energy transfer processes that do not appear in nature or in full three-dimensional scattering calculations. A famous example of a ''false resonance'' is the early prediction[16–19] of resonant features in state-to-state integral cross sections for the $H+H_2$ reaction. Subsequent, more accurate calculations[20–24] revealed that these structures were spurious. A second instance is a feature in reduced-dimensionality quantum scattering calculations for the $O(1D)+H_2\rightarrow OH+H$ reaction at a collision energy of 0.22 eV.[25] This structure does not appear in the results of the full three-dimensional study of Peng *et al.*[26]

For the Ca–He collision (1), we find that the classical transition probability varies greatly with the relative velocity of the perturber v_X and the distance r between the Rydberg electron and the core. This strong variation leads to spurious peaks in state-to-state cross sections. These peaks cannot reflect true resonances, because they are due to features in classical probability that are much narrower than the de Broglie wavelength of an electron moving with a velocity v_X. That is, structures in the classical phase space leading to these energy transfer processes are beyond what the uncertainty principle allows.

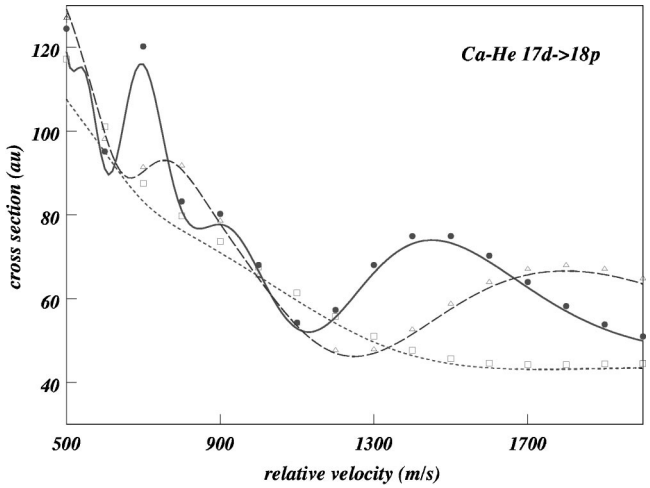

FIG. 1. Partial magnetic cross sections for $17d\rightarrow18p$ transitions in Ca–He collisions. Semiclassical results (points) of Morrison *et al.* (Ref. 3) are compared to the quantum impulse cross sections of Isaacs and Morrison (Ref. 2) (lines) for $|m_0|=0$ (solid line and closed circles), $|m_0|=1$ (long-dashed line and open triangles), and $|m_0|=2$ (short-dashed line and open squares).

The broad theoretical context of the present research, as for the quantal calculations of Isaacs and Morrison[15,2] and the semiclassical study of Morrison *et al.*,[3] is the binary encounter approximation,[11] in which three-body interactions are neglected and the interaction potential for the system—consisting of a Rydberg electron, the core, and a perturber—is approximated by a sum of two-body interactions. We further neglect the explicit core–perturber interaction, relegating the core to the role of a ''spectator'' whose function is to support the (quasifree) initial and final physical states of the Rydberg electron. Within this context we further invoke the Fermi point contact approximation,[1] in which the interaction that governs the binary collision between the electron and the perturber is modeled by a pseudopotential that is proportional to $\delta(\mathbf{r}-\mathbf{R})$, where $\mathbf{r}$ is the position coordinate of the Rydberg electron and $\mathbf{R}$ is that of the perturber. This approximation is valid provided the corresponding cross section depends weakly on the kinetic energy of the Rydberg electron and that the atomic polarizability of the perturber is small—conditions that are well satisfied by the system at hand. The classical equivalent of the Fermi model is the approximation that the electron–perturber encounter occurs only at a single point in space.

Interest in classical treatments of Rydberg states has increased since it became feasible to create in the laboratory mesoscopic atomic states whose evolution can be described classically.[27–30] Although the states of interest in the present application are not this highly excited, recent theoretical work on classical statistical distributions that correspond to quantum-mechanical stationary states[31] is highly relevant to the model we describe. In the context of collisions of ground-state atoms with Rydberg atoms, classical models of angular-momentum mixing,[32] of energy transfer between Rydberg states,[33] and of the inelastic atomic form factor[34]

have illustrated the ability of classical physics, judiciously applied, to explain phenomena not only for quantum numbers large enough to enter the macroscopic realm of the correspondence principle[35] but also for lower-lying Rydberg states, which heretofore had been considered the province of quantal or semi-classical descriptions. It is in the spirit of such recent developments that we offer the present classical analysis of alignment effects in rare-gas collisions with initially aligned Rydberg targets.

In the purely classical theory detailed in Sec. II, we investigate the effect of constraints on the orbital energy $E(n,l)$, the orbital angular momentum $\mathbf{L}$, and the projection of $\mathbf{L}$ on an axis coincident with the initial relative velocity. Specifically, *we constrain these observables to be consistent with their values as calculated from the corresponding quantum-mechanical eigenvalues for initial- and final-state quantum numbers* $\alpha=(n,l,m)$ and $\alpha'=(n',l',m')$. In general, the issue is how such constraints influence the dynamics of transfer from the internal energy of a bound two-body core–satellite (CS) system to the translational energy of a perturber X in the scattering process

$$\mathrm{CS}(\alpha)+X\rightarrow\mathrm{CS}(\alpha')+X. \tag{2}$$

[For the process Eq. (1), the core is the Ca^+ ion, the satellite is the Rydberg electron, and the perturber is the He atom.] In our model, the size of the satellite's orbit about the core is much greater than the region in which the perturber X interacts with the satellite. Under these conditions we may invoke the point contact approximation,[1] according to which energy transfer occurs only when the satellite collides elastically with the perturber at a single point in space.

A simple counting argument illustrates the severity of such constraints. A collision between a satellite S and a perturber X is completely described by the location $\mathbf{r}$ of the point interaction, the velocity $\mathbf{v}_s$ of the satellite, the initial velocity $\mathbf{v}_X$ of the perturber, and the scattering angles $\Omega_i=(\theta_i,\phi_i)$. Thus, in addition to $\mathbf{v}_X=v_X\hat{\mathbf{z}}$, one must specify eight parameters to describe a scattering event. Because in the experimental situations of interest the CS system is oriented symmetrically with respect to the relative velocity of the CS–X collision,[7] one of these parameters is the angle of an arbitrary rotation of the system about the relative velocity. This symmetry consideration leaves only seven dynamically significant parameters. Specification of the initial- and final-state quantum numbers for a transition $(n,l,m)\rightarrow(n',l',m')$ provides six constraints, leaving only one degree of freedom. Thus, for a given electron–core separation r, only a discrete set of trajectories is allowed for a particular state-changing collision. (As we shall see, a maximum of 32 such trajectories exists, corresponding to the roots of an eighth-degree polynomial and the four combinations of signs that specify whether the satellite is moving toward or away from the core before and after the collision.)

While one must turn to quantum-mechanical calculations for quantitative predictions of near-resonance energy transfer, the classical model described in Sec. II offers a qualitative picture that allows one to address such issues as where energy transfer occurs and at what electron speed the collision takes place. Section III presents the technical details needed to implement this model via an expression for the transfer function $T_{\alpha\alpha'}(v_p,r)$, from which one can calculate cross sections that are differential in the final-state quantum numbers

$$\frac{d\sigma_\alpha}{dn'\,dl'\,dm'}=\int T_{\alpha\alpha'}(v_p,r)P_\alpha(r)P_{\alpha'}(r)dr, \tag{3}$$

where $v_p=(m_c+m_s)v_X/m_c$, with m_c and m_s the masses of the core C and satellite S and v_X the relative speed of perturber X and the target. The functions $P_\alpha(r)$ and $P_{\alpha'}(r)$ give the electron probability distribution as a function of the C–S distance. As we shall illustrate in Sec. V, graphs of the transfer function $T_{\alpha\alpha'}$ reveal rich structure due to the spatial constraints imposed by conservation of energy and angular momentum. Section IV presents a systematic procedure for evaluation of the transfer function. Section V presents results for the Ca–He process (1) and compares them to those from prior quantal and semiclassical calculation. Our conclusions follow in Sec. VI.

II. AN ENSEMBLE MODEL OF THREE-BODY COLLISIONS

Our classical picture of near-resonant energy transfer begins in a universe of satellites S orbiting cores C to which they are bound by a central potential $V(r)$. If the potential depends on r as $1/r$, as in the Rydberg-atom rare-gas collision (1), then this is a universe of Kepler orbits. In anticipation of our eventual comparison to quantum mechanics, we imagine that each orbit has total energy $E_\alpha=E(n,l)$, magnitude of angular momentum $L=\sqrt{l(l+1)}\hbar$, and projection of angular momentum along the z axis $L_z=m\hbar$. In this paper we apply our model to an electrostatically bound Rydberg atom and, in a future publication, will do so for a harmonically bound molecule in the rigid-rotor approximation; in this section we shall present results for both systems. Their bound-state energies are

$$E_\alpha=\begin{cases}\dfrac{-\mu_s e^4}{2\hbar^2(n-\delta_l)^2} & \text{Kepler orbit}\\[2ex] \hbar\omega_0(n+\frac{1}{2})+\beta l(l+1) & \text{harmonically bound rigid rotor.}\end{cases} \tag{4}$$

Here, μ_s is the reduced mass of the electron–core system and δ_l is the quantum defect. For the harmonically bound molecule, ω_0 is the natural angular frequency and β is the rotational constant.

To determine the velocity of a satellite and its position with respect to the core, one must specify three degrees of freedom in addition to the aforementioned quantum numbers. For these degrees of freedom we choose the angles shown in Fig. 2. This figure shows an orbit with angular momentum **L**, Runge–Lentz vector **A**, and phase ϕ_t in a coordinate system whose z axis is parallel to the perturber velocity. Here, ϕ_t is the angle from the Runge–Lentz vector to the position of the satellite relative to the core at time t, with $\phi_t=0$ at $t=0$. Because **A** is in the plane of the orbit, its direction can be uniquely specified by a single angle ϕ_c constructed as follows. First, define a vector **C** along the intersection of the plane containing **L** and the z axis with the plane of the orbit; the origin of **C** is at the center of mass. Then, ϕ_c is the angle of the right-handed rotation about **L** that carries **C** to the position vector **r** of the electron. The direction ϕ_A of Runge–Lentz vector can then be found by rotating **C** about **L** through an angle $\phi_A=\phi_c-\phi_t$. For the three degrees of freedom we choose: the azimuthal direction ϕ_L of the angular momentum vector, the direction ϕ_A of the Runge–Lentz vector, and the phase of the orbit, as determined by the time t it takes the satellite to travel from the aphelion of its orbit. Although E, L, and L_z are fixed, ϕ_L and ϕ_A are distributed randomly between 0 and 2π, and t is distributed randomly between 0 and the classical period T of the orbit.

Because E and **L** are conserved, our classical universe, if undisturbed, would remain stable forever. However, our universe also contains randomly distributed perturbing particles X, all of which have velocity $\mathbf{v}_X=v_X\hat{\mathbf{z}}$. Occasionally one of these perturbers strikes a satellite, changing E, L, and L_z of its orbit. We wish to know the distribution in energy and angular momentum of the orbits that have suffered a collision. To find this distribution, we may proceed rigorously from the Boltzmann equation of transport. Because the forms of the resulting cross sections are intuitive, we relegate this detailed analysis to the Appendix and simply state the results here.

If insufficient time has passed to significantly alter the initial distribution of orbits, then the rate of collisions that create new orbits is

$$k_\alpha=\int\int\int\left(\frac{d\sigma}{d\Omega_i}\right)u_r P_\alpha(\mathbf{v}_s,\mathbf{r}_s)d\mathbf{v}_s\,d\mathbf{r}_s\,d\Omega_i. \tag{5}$$

Here, $d\sigma/d\Omega_i$ is the differential cross section for the electron–perturber collision, $u_r=|\mathbf{v}_s-\mathbf{v}_X|$ is the relative speed of the satellite S and perturber X, and $\mathbf{r}_s$ and $\mathbf{v}_s$ are the displacement and velocity, respectively, of the satellite with respect to the core. The function $P_\alpha(\mathbf{v}_s,\mathbf{r}_s)$ is the probability that an electron with initial quantum numbers $\alpha=(n,l,m)$ will have position $\mathbf{r}_s$ and velocity $\mathbf{v}_s$. Finally, Ω_i is the center-of-mass scattering angle of the satellite–perturber collision. By dividing this rate by the speed v_X of the perturber, one obtains the cross section

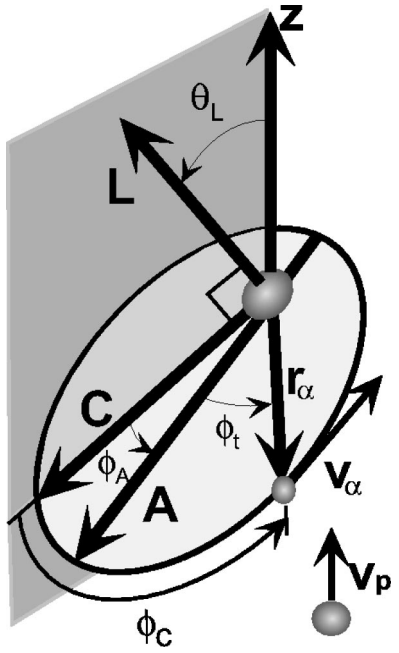

FIG. 2. Parametrization of the velocity $\mathbf{v}_\alpha$ and position $\mathbf{r}_\alpha$ in terms of $\alpha=(n',l',m'),\phi_c$, r, and angular momentum $\hat{L}$.

$$\sigma_\alpha=\frac{1}{v_X}\int\int\int\left(\frac{d\sigma}{d\Omega_i}\right)u_r P_\alpha(\mathbf{v}_s,\mathbf{r}_s)d\mathbf{v}_s\,d\mathbf{r}_s\,d\Omega_i. \tag{6}$$

Within the constraints described above, specification of the initial velocities $\mathbf{v}_s$ and $\mathbf{v}_X$ and of the scattering angle Ω_i completely determines the final velocities $\mathbf{v}_s'$ and $\mathbf{v}_x'$. In the point contact approximation, the final displacement is equal to the initial displacement, that is, $\mathbf{r}_s'=\mathbf{r}_s$. Thus, from $\mathbf{v}_s$, $\mathbf{r}_s$, and Ω_i, we can determine $\mathbf{v}_s'$ and $\mathbf{r}_s'$ and hence the energy and angular momentum of the final state. Moreover, one can write the final quantum numbers n', l', and m' as functions of $\mathbf{v}_s$, $\mathbf{r}_s$, and Ω_i, although the functional forms are by no means simple. In anticipation of our eventual comparison to quantum mechanics, we modify (6) to define a cross section that is differential in the final quantum numbers

$$\begin{aligned}\frac{d\sigma_\alpha}{dn'\,dl'\,dm'}=\frac{1}{v_X}\int\int\int\ &\delta(n'-n'[\mathbf{v}_s,\mathbf{r}_s,\Omega_s])\\ &\times\delta(l'-l'[\mathbf{v}_s,\mathbf{r}_s,\Omega_s])\\ &\times\delta(m'-m'[\mathbf{v}_s,\mathbf{r}_s,\Omega_s])\\ &\times P_\alpha(\mathbf{v}_s,\mathbf{r}_s)u_r\left(\frac{d\sigma}{d\Omega_i}\right)d\mathbf{v}_s\,d\mathbf{r}_s\,d\Omega_i.\end{aligned} \tag{7}$$

We call this quantity a *number differential cross section* and justify its form rigorously in the Appendix.

The number differential cross section is distinct from the conventional classical cross section $\sigma^{(cl)}_{n\,l\,m\to n'l'm'}$ for producing a final state with values of n', l', and m' within one unit of the true final-state quantum numbers.[31] The two cross sections are related by

$$\sigma^{(cl)}_{n\,lm\to n'l'm'}=\frac{1}{V}\int_{\max(m'-\Delta/2,-\hbar\sqrt{l'(l'+1)})}^{\min(m'+\Delta/2,+\hbar\sqrt{l'(l'+1)})}\int_{l'}^{l'+\Delta}\int_{n'}^{n'+\Delta}\frac{d\sigma_\alpha}{dn''dl''dm''}dn''\,dl''\,dm'', \tag{8}$$

where $V\approx 1/\Delta^3$ is the volume of integration and Δ is the binning parameter for Monte Carlo evaluation of the integral. Although details of how bins for the final-state quantum numbers are defined differ depending on the implementation, Δ is normally set equal to 1. (In Sec. V we discuss a numerical comparison of the two definitions which illuminates their relationship.) For quantum numbers much larger than 1, the number differential cross section is likely to vary slowly with n', l', and m'. In this limit, the two cross sections are approximately equal, because the volume of integration is exactly 1. In this paper, however, we are interested in transitions to small values of n', l', and m' for which the cross section varies strongly with these quantum numbers. In this case, the two approaches lead to very different results. We consider the number differential cross section more appropriate to our concerns because it conserves energy, total angular momentum, and angular momentum projection along the quantization axis. We can therefore use the number differential cross section to explore the effect of constraining these observables on a scattering process.

In the next section we reduce the eight-dimensional integral of Eq. (7) to a one-dimensional integral by introducing the transfer function $T_{\alpha\alpha'}(v_p,r)$ of Eq. (3). The complexity of the derivation is not reduced significantly by presupposing a specific mass combination, so no such approximations are made. We encourage readers who are not keen on the details to skip to the step-by-step implementation algorithm in Sec. IV.

III. DETERMINATION OF THE TRANSFER FUNCTION AND NUMBER DIFFERENTIAL CROSS SECTION

A. Reduction of the general three-body point interaction problem to the special case of a core of infinite mass

The algebra required to determine the transfer function $T_{\alpha\alpha'}(v_p,r)$ so that the multidimensional integral in Eq. (7) for the number differential cross section can be reduced to the one-dimensional integral (3) and evaluated is quite involved. To render it more tractable, we first invoke the point contact approximation.[1] In this model the core C acts only as a spectator, so its velocity does not change during the perturber–satellite collision

$$\mathbf{v}_c'=\mathbf{v}_c. \tag{9}$$

Regarding this equality, note that although the collision actually does change the core velocity, it does so on a time scale comparable to the period of the core–satellite rotation. In the point contact approximation, this time scale is much longer than that of the perturber–satellite collision. Therefore, the same model within which the interaction occurs at only one point in space allows us to assume that the energy transfer process takes place without changing the core velocity. After the collision, the satellite's new velocity is $\mathbf{v}_s'$. The postcollision velocities $\mathbf{v}_c$ and $\mathbf{v}_s'$ correspond to the initial conditions of a different orbit, with altered relative energy, angular momentum, *and* center-of-mass velocity.

Using the equality (9) and conservation of total linear momentum, we can recast the general problem of three arbitrary masses m_s, m_c, and m_x that collide with relative speed v_X into the simpler problem of the collision of a perturber of mass m_p and speed v_p with a satellite of mass μ_s that orbits a stationary core of infinite mass. This derivation exploits the fact that the motion of the core is unaffected by the collision. We emphasize that no additional approximations are made by recasting the problem in this way.

In a reference frame in which the center of mass of the CS system is stationary before the collision, the velocities $\mathbf{v}_c$ and $\mathbf{v}_s$ are related to their relative velocity

$$\mathbf{v}=\mathbf{v}_s-\mathbf{v}_c, \tag{10a}$$

by

$$\mathbf{v}_s=\frac{m_c}{m_c+m_s}\mathbf{v}, \tag{10b}$$

$$\mathbf{v}_c=-\frac{m_s}{m_c+m_s}\mathbf{v}. \tag{10c}$$

Clearly, Eqs. (10a)–(10c) are consistent with the use of a reference frame in which the initial center-of-mass velocity of the core–satellite system is zero

$$\mathbf{p}_c+\mathbf{p}_s=m_s\mathbf{v}_s+m_c\mathbf{v}_c \tag{11a}$$

$$=\frac{m_cm_s-m_cm_s}{m_c+m_s}\mathbf{v} \tag{11b}$$

$$=0. \tag{11c}$$

A collision with the perturber rotates the relative velocity $\mathbf{u}_r=\mathbf{v}_s-\mathbf{v}_X$ of the perturber and satellite so that the final satellite velocity is

$$\mathbf{v}_s'=\mathbf{v}_X+\frac{m_s}{m_s+m_x}\mathbf{u}_r+\frac{m_x}{m_x+m_s}\mathsf{R}_i\,\mathbf{u}_r \tag{12a}$$

$$=\frac{m_c}{m_c+m_s}\left[\frac{m_s\mathbf{v}+m_x\mathbf{v}_p}{m_s+m_x}+\frac{m_x}{m_x+m_s}\mathsf{R}_i(\mathbf{v}-\mathbf{v}_p)\right], \tag{12b}$$

where R_i is a rotation matrix, unconstrained by conservation of energy or angular momentum, that is determined by the dynamics of a single collision. In this equation we have also introduced the effective perturber velocity

$$\mathbf{v}_p=\frac{m_c+m_s}{m_c}\mathbf{v}_X. \tag{13}$$

To evaluate the energy and angular momentum of the final state, it is more useful to know the relative velocity than the velocity of the satellite alone. Fortunately, because of the spectator assumption of (9), the relative velocity is easily obtained as

$$\mathbf{v}' = \mathbf{v}_s' - \mathbf{v}_c \tag{14a}$$

$$= \mathbf{v}_p + \frac{\mu_s}{m_p+\mu_s}\mathbf{v}_r + \frac{m_p}{m_p+\mu_s}\,\mathsf{R}_i\mathbf{v}_r\,, \tag{14b}$$

where we have made the substitutions

$$\mathbf{v}_r = \mathbf{v} - \mathbf{v}_p = \frac{m_c+m_s}{m_s}(\mathbf{v}_s - \mathbf{v}_X), \tag{14c}$$

$$m_p = \frac{m_c^2 m_x}{(m_c+m_s)(m_c+m_s+m_x)}, \tag{14d}$$

and

$$\mu_s = \frac{m_s m_c}{m_s+m_c}. \tag{14e}$$

Care must be exercised in using Eq. (14a). This equation gives correctly the relative velocity of the satellite and the core, but the relationship between the relative and satellite–core velocities *after the collision* is not trivial. In particular, because $\mathbf{p}_c+\mathbf{p}_s\neq 0$, we cannot use relationships analogous to Eqs. (10b); i.e.,

$$\mathbf{v}_s' \neq \frac{m_c}{m_c+m_s}\mathbf{v}', \tag{15a}$$

$$\mathbf{v}_c' \neq -\frac{m_s}{m_c+m_s}\mathbf{v}'. \tag{15b}$$

Fortunately, the energy and angular momentum of the final state depend on the relative velocity, not on $\mathbf{v}_s'$ or $\mathbf{v}_c'$.

Because Eq. (14a) is structurally identical to Eq. (12a), we can easily transform from the general case of three arbitrary masses to a core of infinite mass. The transformation is made complete by recognizing that neither the relative energy of the collision nor the structure of (7) is changed by the substitution of hypothetical masses μ_s and m_p and velocities $\mathbf{v}$, $\mathbf{v}_p$, and $\mathbf{v}_r$ for the physical masses m_c, m_s, and m_x, and the physical velocities $\mathbf{v}_c$, $\mathbf{v}_s$, $\mathbf{v}_X$, and $\mathbf{u}_r$. The relative kinetic energy becomes

$$E_{\rm rel} = \frac{1}{2}\frac{m_s m_x}{m_s+m_x}u_r^2 = \frac{1}{2}\frac{m_s m_x}{m_s+m_x}(\mathbf{v}_s-\mathbf{v}_X)^2 \tag{16a}$$

$$= \frac{1}{2}\frac{\mu_s m_p}{\mu_s+m_p}v_r^2 = \frac{1}{2}\frac{\mu_s m_p}{\mu_s+m_p}(\mathbf{v}-\mathbf{v}_p)^2, \tag{16b}$$

and the number differential cross section (7) becomes

$$\frac{d\sigma_\alpha}{dn'\,dl'\,dm'} = \frac{1}{v_p}\int\int\int \delta(n'-n'[\mathbf{v},\mathbf{r},\Omega])\times\delta(l'-l'[\mathbf{v},\mathbf{r},\Omega])\,\delta(m'-m'[\mathbf{v},\mathbf{r},\Omega])\times P_\alpha(\mathbf{v},\mathbf{r})\,v_r\left(\frac{d\sigma}{d\Omega_i}\right)d\mathbf{v}\,d\mathbf{r}\,d\Omega_i\,. \tag{17}$$

This step completes the simplification resulting from the point contact approximation and conservation of linear momentum. From this point on, we assume a satellite of mass μ_s orbiting a core of infinite mass with velocity $\mathbf{v}$ which is struck by a perturber of mass m_p moving with a speed v_p. To apply the results of this simplified situation to the general case (without approximation), we merely make the substitutions of Eqs. (10), (13), (14c), (14d), and (14e).

B. Distribution of the initial velocity and displacement vectors

To derive an expression for the initial electron probability $P_\alpha(\mathbf{v},\mathbf{r})$, we first determine $\mathbf{r}(E,L,L_z;\phi_L,\phi_A,t) = \mathbf{r}_\alpha(\phi_L,\phi_A,t)$ and $\mathbf{v}(E,L,L_z;\phi_L,\phi_A,t)=\mathbf{v}_\alpha(\phi_L,\phi_A,t)$. The semicolons in the arguments of these quantities signify that while the values of E, L, and L_z are the same for every orbit in our ensemble, ϕ_L, ϕ_A, and t are distributed randomly.

Letting θ_L and ϕ_L be the spherical polar coordinates of $\mathbf{L}$, with

$$\cos\theta_L = \frac{L_z}{L} = \frac{m}{\sqrt{l(l+1)}}, \tag{18}$$

we find

$$\mathbf{r}_\alpha(\phi_L,\phi_A,t) = \mathbf{r}_\alpha(\phi_L,\phi_c-\phi_t,r) \tag{19a}$$

$$= r(t)\begin{pmatrix} c\theta_L\,c\phi_L\,c\phi_c - s\phi_L\,s\phi_c \\ c\theta_L\,s\phi_L\,c\phi_c + c\phi_L\,s\phi_c \\ -s\theta_L\,c\phi_c \end{pmatrix}, \tag{19b}$$

where we have used the shorthand notations $c\theta\equiv\cos\theta$ and $s\theta\equiv\sin\theta$ and where $r(t)$ is the distance of the satellite S from the core C at time t as determined from Newton's laws. It is significant that the only functional dependence of $\mathbf{r}_\alpha(\phi_L,\phi_c,r)$ on ϕ_A is through the variable ϕ_c. Because ϕ_A is assumed to be uniformly distributed from 0 to 2π, the distribution of values of ϕ_c is also uniform. (This is true even though the distribution of ϕ_t favors angles close to 0 and π.) It is therefore advantageous to define the direction of the Runge–Lentz vector in terms of ϕ_c rather than ϕ_A.

To determine the electron velocity $\mathbf{v}_\alpha(\phi_L,\phi_c,r)$, we first express this quantity in terms of its components parallel and perpendicular to $\mathbf{r}_\alpha(\phi_L,\phi_c,r)$, as

$$\mathbf{v}_\alpha(\phi_L,\phi_c,r) = v_{\alpha r}\hat{r}_\parallel + v_{\alpha\perp}\hat{r}_\perp\,, \tag{20a}$$

where

$$\hat{r}_\parallel = \frac{\mathbf{r}_\alpha(\phi_L,\phi_c,r)}{r} = \begin{pmatrix} c\theta_L\,c\phi_L\,c\phi_c - s\phi_L\,s\phi_c \\ c\theta_L\,s\phi_L\,c\phi_c + c\phi_L\,s\phi_c \\ -s\theta_L\,c\phi_c \end{pmatrix}, \tag{20b}$$

and

$$\hat{r}_\perp = \frac{\mathbf{r}_\alpha\left(\phi_L,\phi_c+\frac{\pi}{2},r\right)}{r} = \begin{pmatrix} -c\theta_L\,c\phi_L\,s\phi_c - s\phi_L\,c\phi_c \\ -c\theta_L\,s\phi_L\,s\phi_c + c\phi_L\,c\phi_c \\ s\theta_L\,s\phi_c \end{pmatrix}. \tag{20c}$$

The perpendicular component of $\mathbf{v}_\alpha(\phi_L,\phi_c,r)$ is determined from the angular momentum of the initial state as

$$\mathbf{L}=|\mu_s\mathbf{r}_\alpha(\phi_L,\phi_c,r)\times\mathbf{v}_\alpha(\phi_L,\phi_c,r)| \tag{21a}$$

$$=|\mu_s r\hat{r}_\parallel\times(v_{\alpha r}\hat{r}_\parallel+v_{\alpha\perp}\hat{r}_\perp)| \tag{21b}$$

$$=\mu_s v_{\alpha\perp} r\hat{L}. \tag{21c}$$

From (21a), we conclude that this component of the velocity is

$$v_{\alpha\perp}=\frac{\sqrt{l(l+1)}\hbar}{\mu_s r}. \tag{22}$$

From conservation of energy, we know that speed $v_\alpha=\sqrt{v_{\alpha r}^2+v_{\alpha\perp}^2}$ of the satellite is

$$v_\alpha=\sqrt{\frac{2[E(n,l)-V(r)]}{\mu_s}}, \tag{23}$$

so that the radial component of the velocity $\mathbf{v}_\alpha$ is

$$v_{\alpha r}=k\sqrt{\frac{2[E(n,l)-V(r)]}{\mu_s}-\frac{l(l+1)\hbar^2}{\mu_s^2 r^2}}. \tag{24}$$

In the last expression we introduced the index k, which is equal to ±1 acccordingly as the satellite is receding from or approaching the core: $k(t)=-1$ for $0<t<T/2$ and $k(t)=+1$ for $T/2<t<T$. This analysis yields for the electron velocity the following explicit expression:

$$\mathbf{v}_\alpha(\phi_L,\phi_c,r)$$
$$=\frac{\sqrt{l(l+1)}\hbar}{\mu_s r}\begin{pmatrix}-c\theta_L\,c\phi_L\,s\phi_c-s\phi_L\,c\phi_c\\-c\theta_L\,s\phi_L\,s\phi_c+c\phi_L\,c\phi_c\\s\theta_L\,s\phi_c\end{pmatrix}$$
$$+k\sqrt{\frac{2[E(n,l)-V(r)]}{\mu_s}-\frac{l(l+1)\hbar^2}{\mu_s^2 r^2}}$$
$$\times\begin{pmatrix}c\theta_L\,c\phi_L\,c\phi_c-s\phi_L\,s\phi_c\\c\theta_L\,s\phi_L\,c\phi_c+c\phi_L\,s\phi_c\\-s\theta_L\,c\phi_c\end{pmatrix}. \tag{25}$$

Equations (19a) and (25) give the position and velocity of the satellite for initial state α and parameters ϕ_L,ϕ_c, and t. To find the probability $P_\alpha(\mathbf{v},\mathbf{r})$, we need only convolve the uniform distribution functions over these variables with Dirac delta functions that enforce Eqs. (19a) and (25)

$$P_\alpha(\mathbf{v},\mathbf{r})=\frac{1}{4\pi^2 T}\int_0^{2\pi}\int_0^{2\pi}\int_0^{T}\delta^3(\mathbf{r}-\mathbf{r}_\alpha(\Omega_L,\phi_c,t))$$
$$\times\delta^3(\mathbf{v}-\mathbf{v}_\alpha(\Omega_L,\phi_c,t))\,d\phi_L\,d\phi_c\,dt. \tag{26}$$

Considerable effort has been expended in determining explicit forms of the distribution function $P_\alpha(\mathbf{v},\mathbf{r})$ for a Rydberg orbital.[31] For our purposes, however, the integral form (26) will suffice, so we need not explicitly evaluate this function.

C. The transfer function as a one-dimensional integral over a delta function

We now substitute Eq. (26) for $P_\alpha(\mathbf{v},\mathbf{r})$ into the definition (17) of the number differential cross section. Changing the order of integration and integrating over $\mathbf{v}$ and $\mathbf{r}$, we find

$$\frac{d\sigma_\alpha}{dn'\,dl'\,dm'}=\frac{1}{4\pi^2 T v_p}\int_0^T\int_0^{2\pi}\int_0^{2\pi}\int\delta(n'-n'[\phi_L,\phi_c,r,k,\Omega_i])\,\delta(l'-l'[\phi_L,\phi_c,r,k,\Omega_i])$$
$$\times\delta(m'-m'[\phi_L,\phi_c,r,k,\Omega_i])\,v_r\left(\frac{d\sigma}{d\Omega_i}\right)d\Omega_i\,d\phi_L\,d\phi_c\,dt. \tag{27}$$

The factor of $1/4\pi^2 T$ results from the uniformity of the distribution of t, ϕ_c, and ϕ_L, with values of $1/T$, $1/2\pi$, and $1/2\pi$, respectively.

It is convenient to change the variable of integration from time t to the core–satellite distance r. In so doing, we must take into account that each value of r corresponds to two values of t. Dividing the integration over t into two parts—one for the satellite approaching the core, the other for it receding—we obtain

$$\frac{d\sigma_\alpha}{dn'\,dl'\,dm'}=\frac{1}{8\pi^2 v_p}\sum_{k=\pm1}\int_{r_{mn}}^{r_{mx}}\int_0^{2\pi}\int_0^{2\pi}\int\delta(n'-n'[\phi_L,\phi_c,r,k,\Omega_i])\,\delta(l'-l'[\phi_L,\phi_c,r,k,\Omega_i])$$
$$\times\delta(m'-m'[\phi_L,\phi_c,r,k,\Omega_i])P_\alpha(r)\,v_r\left(\frac{d\sigma}{d\Omega_i}\right)d\Omega_i\,d\phi_L\,d\phi_c\,dr, \tag{28}$$

where r_{mn} and r_{mx} are the inner and outer classical turning points, respectively, and $P_\alpha(r)$ is the *classical* probability of finding the electron at a distance r from the core. For the two cases under examination, this classical probability is

$$P_\alpha(r)=\frac{2}{T_\alpha}\frac{1}{|v_{\alpha r}|} \tag{29a}$$

$$=\begin{cases}\dfrac{1}{\pi(n-\delta_l)^3\dfrac{\hbar^3}{\mu_s e^4}\sqrt{\dfrac{-l(l+1)\hbar^2}{\mu_s^2 r^2}+\dfrac{2e^2}{\mu_s r}-\dfrac{e^4}{\hbar^2(n-\delta_l)^2}}} & \text{Rydberg electron}\\ \dfrac{\omega_0}{\pi\sqrt{\dfrac{-l(l+1)\hbar^2}{\mu_s^2 r^2}+\dfrac{2[\hbar\omega_0(n+\frac{1}{2})+\beta l(l+1)]}{\mu_s}-\omega_0^2(r-r_0)^2}} & \text{harmonic oscillator.}\end{cases} \tag{29b}$$

A semiclassical variant of our model could be obtained by replacing this classical probability by its quantum-mechanical counterpart. We shall examine this alternative in Sec. V.

From symmetry arguments, one can see that the integrand of (28) does not depend on the azimuthal angle ϕ_L. So we can reduce the number differential cross section to a four-dimensional integral over three delta functions

$$\frac{d\sigma_\alpha}{dn'\,dl'\,dm'}=\frac{1}{4\pi v_p}\sum_{k=\pm 1}\int_{r_{mn}}^{r_{mx}}\int_0^{2\pi}\int \delta(n'-n'[\phi_c,r,k,\Omega_i])\,\delta(l'-l'[\phi_c,r,k,\Omega_i])$$

$$\times\,\delta(m'-m'[\phi_c,r,k,\Omega_i])\,P_\alpha(r)v_r\left(\frac{d\sigma}{d\Omega_i}\right)d\Omega_i\,d\phi_c\,dr. \tag{30}$$

We now turn to the remaining integrations. We first evaluate the effect of scattering a satellite with initial velocity $\mathbf{v}=\mathbf{v}_\alpha[\phi_L,\phi_c,r,k,\Omega_i]$ at position $\mathbf{r}=\mathbf{r}_\alpha[\phi_L,\phi_c,r,k,\Omega_i]$ by a perturber with velocity $\mathbf{v}_p=v_p\hat{\mathbf{z}}$ through scattering angles $\Omega_i=(\theta_i,\phi_i)$. The center-of-mass scattering angle θ_i is unambiguously defined as the angle between the initial relative velocity $\mathbf{v}-\mathbf{v}_p$ and the final relative velocity $\mathbf{v}'-\mathbf{v}_p'$. We define the azimuthal scattering angle ϕ_i to be the dihedral angle between final relative velocity and the plane containing both $\mathbf{v}_p$ and $\mathbf{v}-\mathbf{v}_p$. We can then find the final velocity of the electron $\mathbf{v}'$ from the rotated relative velocity of the collision by applying Eq. (14a). From $\mathbf{v}'$ we can find the final energy E', magnitude of angular momentum L', and component of angular momentum in the $\hat{\mathbf{z}}$ direction L_z' as functions of ϕ_c, r, k, and Ω_i, and in turn, the final quantum numbers n', l', and m'. Rather than deal with explicit expressions for n', l', and m', it is (much) more convenient to use the related quantities

$$\Delta\omega=\frac{E_{\alpha'}-E_\alpha}{\hbar} \tag{31a}$$

$$=\begin{cases}\dfrac{\mu_s e^4}{\hbar^3}\left[\dfrac{1}{2(n-\delta_l)^2}-\dfrac{1}{2(n'-\delta_{l'})^2}\right] & \text{Rydberg electron}\\ \omega_0(n'+\frac{1}{2})+\dfrac{\beta'}{\hbar}l'(l'+1)-\omega_0(n+\frac{1}{2})-\dfrac{\beta}{\hbar}l(l+1) & \text{harmonic oscillator,}\end{cases} \tag{31b}$$

$$\Delta\lambda=\frac{\mu_s\mathbf{r}\cdot(\mathbf{v}_\alpha'-\mathbf{v}_\alpha)}{\hbar} \tag{32a}$$

$$=\frac{\mu_s r}{\hbar}\left[k'\sqrt{\frac{2[E_\alpha'-V(r)]}{\mu_s}-\frac{l'(l'+1)\hbar^2}{\mu_s^2 r^2}}-k\sqrt{\frac{2[E_\alpha-V(r)]}{\mu_s}-\frac{l(l+1)\hbar^2}{\mu_s^2 r^2}}\right], \tag{32b}$$

and

$$\Delta m^{=}(m'-m). \tag{33}$$

These quantities enable us to separate the dependence of the final state on $\mathbf{v}_\alpha$ and $\mathbf{r}_\alpha$ from its dependence on the scattering angles θ_i and ϕ_i, *viz.*,

$$\begin{pmatrix}\Delta\omega\\ \Delta\lambda\\ \Delta m\end{pmatrix}=\mathbf{A}\begin{pmatrix}\sin\theta_i\cos\phi_i\\ \sin\theta_i\sin\phi_i\\ \cos\theta_i-1\end{pmatrix}=\mathbf{A}\left(\mathbf{w}-\begin{pmatrix}0\\0\\1\end{pmatrix}\right). \tag{34}$$

In this expression, the three-component vector $\mathbf{w}$ is defined as

$$\mathbf{w}=\begin{pmatrix}\sin\theta_i\cos\phi_i\\ \sin\theta_i\sin\phi_i\\ \cos\theta_i\end{pmatrix}. \tag{35}$$

The matrix A depends on the initial experimental conditions, which in this model are described by the variables m_p, μ_s, r, v_p, n, l, m, and ϕ_c. Specifically, this matrix is given by

$$A=\frac{m_p}{\mu_s+m_p}\begin{pmatrix} \dfrac{-\mu_s v_p v_{\alpha\rho}}{\hbar} & 0 & \dfrac{\mu_s}{\mu_s+m_p}\dfrac{\mu_s v_r^2}{\hbar}+\dfrac{\mu_s v_p(v_{\alpha z}-v_p)}{\hbar} \\ \dfrac{\mu_s[(v_{\alpha z}-v_p)(r\,v_{\alpha r}-z\,v_{\alpha z})-z\,v_{\alpha\rho}^2]}{v_{\alpha\rho}\hbar} & \dfrac{-m\,v_r}{v_{\alpha\rho}} & \dfrac{\mu_s(r\,v_{\alpha r}-z\,v_p)}{\hbar} \\ \dfrac{m(v_{\alpha z}-v_p)}{v_{\alpha\rho}} & \dfrac{\mu_s v_r(r\,v_{\alpha r}-z\,v_{\alpha z})}{v_{\alpha\rho}\hbar} & m \end{pmatrix}. \tag{36}$$

The matrix $\mathbf{A}$ contains the additional quantities

$$v_{\alpha z}=-v_\alpha\cos(\beta+\phi_c)\sin\theta_L, \tag{37a}$$

$$v_{\alpha\rho}=v_\alpha\sqrt{1-\cos^2(\beta+\phi_c)\sin^2\theta_L}, \tag{37b}$$

$$z=-r\sin\theta_L\cos\phi_c. \tag{37c}$$

The angle θ_L is the spherical polar angle given by Eq. (18), and β is the angle defined by

$$\cos\beta=\frac{v_{\alpha r}}{v_\alpha}=k\sqrt{1-\frac{l(l+1)\hbar^2}{2[E_\alpha-V(r)]\mu_s r^2}}, \tag{37d}$$

$$\sin\beta=\sqrt{1-\cos^2\beta}. \tag{37e}$$

Operationally, it is useful to express the quantities v_r, $v_{\alpha r}$, and m in the matrix A in terms of v_p, v_α, θ_L, β, and ϕ_c, as

$$v_r=\sqrt{v_\alpha^2+v_p^2+2v_\alpha v_p\cos(\beta+\phi_c)\sin\theta_L}, \tag{37f}$$

$$v_{\alpha r}=v_\alpha\cos\beta, \tag{37g}$$

$$m=\frac{\mu_s r v_\alpha}{\hbar}\cos\theta_L\sin\beta. \tag{37h}$$

These substitutions render all the variables in A independent of one another, an important simplification for the evaluation of expressions involving this important matrix. Note that for a forward-scattered satellite, no exchange of momentum occurs between the satellite and perturber. In this case, the vector $(w_x,w_y,w_z-1)=(\sin\theta_i\cos\phi_i,\sin\theta_i\sin\phi_i,\cos\theta_i-1)$ vanishes, and $\Delta\omega$, $\Delta\lambda$, and Δm become zero as required.

We could, of course, invert Eqs. (31a), (32a), and (33) to obtain the final quantum numbers. A preferable approach, however, is to change the delta functions from (n',l',m') space to $(\Delta\omega,\Delta\lambda,\Delta m)$ space, as

$$\begin{aligned}&\delta(n'-n'[\phi_c,r,k,\Omega_i])\,\delta(l'-l'[\phi_c,r,k,\Omega_i])\\&\quad\times\delta(m'-m'[\phi_L,\phi_c,r,k,\Omega_i])\\&\quad=\delta(\Delta\omega-\Delta\omega[\phi_c,r,k,\Omega_i])\,\delta(\Delta\lambda-\Delta\lambda[\phi_c,r,k,\Omega_i])\\&\qquad\times\delta(\Delta m-\Delta m[\phi_c,r,k,\Omega_i])\frac{\partial(\Delta\omega,\Delta\lambda,\Delta m)}{\partial(n',l',m')},\end{aligned} \tag{38}$$

where the Jacobian is

$$\begin{aligned}\frac{\partial(\Delta\omega,\Delta\lambda,\Delta m)}{\partial(n',l',m')}&=\begin{vmatrix}\dfrac{(l'+\frac{1}{2})\hbar}{\mu_e r\,v'_{\alpha r}} & \dfrac{\partial_{n'}E_{\alpha'}}{\hbar}\end{vmatrix}\\&=\eta\frac{\pi(l'+\frac{1}{2})\hbar}{\mu_e r}P_{\alpha'}(r).\end{aligned} \tag{39}$$

The parameter η depends on the period T' and energy E' of the final state, as

$$\eta=\left|\frac{T'\,\partial_{n'}E_{\alpha'}}{2\pi\hbar}\right|. \tag{40}$$

For both Kepler orbits and the harmonically bound rigid rotor, $\eta=1$.

With this substitution, the number differential cross section becomes

$$\begin{aligned}\frac{d\sigma_\alpha}{dn'\,dl'\,dm'}=\frac{\eta(l'+\frac{1}{2})\hbar}{4\mu_s v_p}\sum_{k=\pm1}\int_0^\infty\int\int_{r_{mn}}^{r_{mx}}\int_0^{2\pi}&\delta(\Delta\omega-\Delta\omega[\phi_c,r,k,\Omega_i])\,\delta(\Delta\lambda-\Delta\lambda[\phi_c,r,k,\Omega_i])\\&\times\delta(\Delta m-\Delta m[\phi_c,r,k,\Omega_i])\,\delta(w'^2-1)P_\alpha(r)P_{\alpha'}(r)\frac{v_r}{r}\left(\frac{d\sigma}{d\Omega_i}\right)2w'^2\,d\phi_c\,dr\,d\Omega_i\,dw'.\end{aligned} \tag{41}$$

In addition to replacing the delta functions, we have added an integration over a dummy variable w'. Without affecting the value of the integral, this additional integration allows us to switch from a spherical polar integration over $w'^2\,d\Omega_i\,dw'$ to a Cartesian integration with volume element $d^3\mathbf{w}=dw_x\,dw_y\,dw_z$. We can then use Eq. (34) to evaluate the integral over $d^3\mathbf{w}$, obtaining

$$\frac{d\sigma_\alpha}{dn'\,dl'\,dm'} = \frac{\eta(l'+\frac{1}{2})\hbar}{2\mu_s v_p}\sum_{k=\pm1}\sum_{k'=\pm1}\int_{r_{mn}}^{r_{mx}}\int_0^{2\pi}\frac{1}{|\det A|} \times \delta(w^2-1)P_\alpha(r)P_{\alpha'}(r)\frac{v_r}{r}\left(\frac{d\sigma}{d\Omega_i}\right)\,d\phi_c\,dr, \tag{42}$$

where w^2 is the square magnitude of the vector $\mathbf{w}$ given, according to Eq. (35), by

$$\mathbf{w}=A^{-1}\begin{pmatrix}\Delta\omega\\ \Delta\lambda\\ \Delta m\end{pmatrix}+\begin{pmatrix}0\\0\\1\end{pmatrix}. \tag{43}$$

The summation over k' accommodates final states in which the satellite either approaches or recedes from the core. This integral can now be recast in the form of Eq. (3) by defining the transfer function

$$T_{\alpha\alpha'}(v_p,r)\equiv\frac{\eta(l'+\frac{1}{2})\hbar}{2\mu_s v_p r}\sum_{k=\pm1}\sum_{k'=\pm1}\int\frac{1}{|\det A|}\delta(w^2-1) \times v_r\left(\frac{d\sigma}{d\Omega_i}\right)\,d\phi_c. \tag{44}$$

An algorithm for evaluating the integral in (44) is presented in Sec. IV.

D. The reaction polynomials

The values of ϕ_c for which the term w^2-1 appears in the delta function in Eq. (44) are the key to reconstructing the trajectory of a state-to-state collision that has occurred at a C–S separation r. To obtain such a trajectory from r, v_p, (n,l,m) and (n',l',m'), we first determine the values of ϕ_c at which w^2-1 vanishes. From this we find the initial velocity $\mathbf{v}$ and the displacement $\mathbf{r}$, within an arbitrary rotation of the system by ϕ_L, by applying Eqs. (19a) and (25). We evaluate the scattering angles Ω_i of the trajectory from Eqs. (43) and (35), and then the final velocities $\mathbf{v}'$ and $\mathbf{v}_p'$. These steps narrow the collision to a handful of allowed trajectories.

To find the values of ϕ_c of these trajectories we now derive an explicit expression for w^2-1. Using Kramer's rule to find $\mathbf{w}$ from Eq. (34), then simplifying the result (extensively), we obtain

$$w^2-1=\begin{cases}\left(\dfrac{m_p}{m_p+\mu_s}\right)^4\dfrac{\mu_s^2v_r^4}{(\hbar\,\det A)^2}G & m\neq0\ \text{or}\ m'\neq0\\ \left(\dfrac{m_p}{m_p+\mu_s}\right)^4\dfrac{\mu_s^2v_r^4\sin^2\phi_c}{(\hbar\,\det A)^2}G_0 & m=m'=0,\end{cases} \tag{45a}$$

where

$$\det A=[\rho_p(1-\cos^2\phi_a\sin^2\theta_L)+\rho_\alpha\sin\beta\sin\theta_L\sin\phi_c] \times\frac{(m_p\mu_s)^3}{(m_p+\mu_s)^6}\left(\frac{r^2v_r^3}{\hbar^3}\right). \tag{45b}$$

The momenta in this expression are

$$\rho_\alpha=\mu_s v_\alpha=\sqrt{2\mu_s[E_\alpha-V(r)]}, \tag{45c}$$

and

$$\rho_b=m_pv_p, \tag{45d}$$

and the functions $G(\theta_L,\phi_c)$ and $G_0(\theta_L,\phi_c)$ are

$$G(\theta_L,\phi_c)=\left(\sum_{i=0}^4 a_i(\sin\theta_L\sin\phi_c)^i\right)+\sin\theta_L\cos\phi_c \times\left(\sum_{i=0}^3 b_i(\sin\theta_L\sin\phi_c)^i\right), \tag{45e}$$

$$G_0(\theta_L,\phi_c)=\frac{G\left(\theta_L=\dfrac{\pi}{2},\phi_c\right)}{\sin^2\phi_c} =\left(\sum_{i=0}^2 c_i\sin^i\phi_c\right)+\cos\phi_c\left(\sum_{i=0}^1 d_i\sin^i\phi_c\right). \tag{45f}$$

Notice that w^2-1 does not vanish at $\phi_c=0$. Table I contains the coefficients a_i and b_i of the function $G(\theta_L,\phi_c)$ and Table II the coefficients c_i and d_i. Provided $G(\theta_L,\phi_c)$ has no roots in common with $|\det A|^2$, the quantity w^2-1 vanishes at the zeros ϕ_c of $G(\theta_L,\phi_c)$. We evaluate these zeros as the roots of the eighth-order ''reaction polynomial''

$$R_{xn}(x)=\left(\sum_{i=0}^4 a_ix^i\right)^2-(\sin^2\theta_L-x^2)\left(\sum_{i=0}^3 b_ix^i\right)^2. \tag{46a}$$

For $m=m'=0$, the function $G_0(\theta_L,\phi_c)$ can be expressed as the series

$$R_{xn}^0(x)=\left(\sum_{i=0}^2 c_ix^i\right)^2-(1-x^2)\phi_c\left(\sum_{i=0}^1 d_ix^i\right)^2. \tag{46b}$$

The roots of $R_{xn}(x_i)$ and $R_{xn}^0(x_i)$ give the values of $\sin\theta_L\sin\phi_c$ for the allowed trajectories for a transition $(n,l,m)\rightarrow(n'l'm')$. One can determine the corresponding values of ϕ_c by evaluating $G(\theta_L,\phi_c)$ or $G_0(\theta_L,\phi_c)$ at $\phi_c=\arcsin(x_i/\sin\theta_L)$ and at $\phi_c=\pi-\arcsin(x_i/\sin\theta_L)$ and choosing the angle for which w^2-1 vanishes. It is then relatively straightforward to determine the transfer function from

$$T_{\alpha\alpha'}(v_p,r)=\left[\frac{\eta(l'+\frac{1}{2})r}{2}\right]\sum_{k=\pm1}\sum_{k'=\pm1}\sum_{\phi_{c,i}}\frac{1}{|\partial_{\phi_c}G|} \times\left|\left[1-\cos^2\phi_c\sin^2\theta_L +\left(\frac{\rho_\alpha}{\rho_p}\right)\sin\beta\sin\theta_L\sin\phi_c\left(\frac{d\sigma}{d\Omega_i}\right)\right]\right|_{\phi_{c,i}}. \tag{47}$$

For the special case $m=m'=0$, the quantity $|\partial_{\phi_c}G|$ should be replaced with $\sin^2\phi_c|\partial_{\phi_c}G_0|$.

TABLE I. Coefficients a_i and b_i for the evaluation of $G(\theta_L,\phi_c)$ and R_{xn} can be generated by multiplying each table entry by $(r^2\mu_s^2/\hbar^3M^2)$.

i	$a_i(\hbar^3M^2/r^2\mu_s^2)$	$b_i(\hbar^3M^2/r^2\mu_s^2)$
0	$2\,\rho_p^2\,\rho\,(\mu_s)r\,c\theta^3+[\Delta^2\,c\theta^2\,\rho_p^2+\rho^2(M)]\hbar$	$-2\Delta\lambda\rho(M)\rho_p\hbar c\theta$
1	$2\rho_\alpha\rho_p\,\rho(\mu_s-m_p)r\,c\theta\,s\beta+2\rho_p\rho_\alpha s\beta\,(\Delta m^2+\Delta\lambda^2\,c\theta^2)\hbar$	$2\Delta\lambda\rho_p^2\rho_\alpha r\,s\beta\,c\theta^2$
2	$2(\rho_p^2(2\,\rho(\mu_s)-\rho_\alpha s\beta\,\Delta m)r\,c\theta+m_p\Delta\omega\,\rho_\alpha^2r^2s\beta^2)$ $+(\Delta^2\rho_p^2+\Delta\lambda^2s\beta^2\rho_\alpha^2+(\Delta\lambda c\beta\,\rho_\alpha-M\,r\,\Delta\omega)^2)\hbar$	$2\Delta\lambda\rho_p(\rho_\alpha^2r\,s\beta^2$ $+(M\,r\,\Delta\omega-\Delta\lambda\rho_\alpha c\beta)\hbar)$
3	$2\rho_p\rho_\alpha s\beta[\Delta\lambda\,c\beta\,\rho_\alpha\,r+r^2(m_p-\mu_s)\Delta\omega+\Delta\lambda^2\hbar]$	$2\Delta\lambda\,\rho_p^2\rho_\alpha\,r\,s\beta$
4	$2\rho_p^2r(c\beta\,\Delta\lambda\rho_\alpha-r\,\Delta\omega\,\mu_s)$	

$$\rho(\gamma)=\rho_\alpha(\Delta m\,s\beta+\Delta\lambda\,c\beta c\theta)-\gamma r\,\Delta\omega\,c\theta,$$
$$M=m_p+\mu_s,\quad c\theta=\cos\theta_L,\quad s\beta=\sin\beta,\quad c\beta=\cos\beta,\quad \Delta^2\equiv\Delta\lambda^2+\Delta m^2$$

IV. SYSTEMATIC EVALUATION OF THE ENERGY TRANSFER FUNCTION

We present here a step-by-step procedure for evaluating the transfer function $T_{\alpha,\alpha'}$ from the initial state $\alpha=(n,l,m)$, the final state $\alpha=(n',l',m')$, the relative velocity v_X between the CS system and the perturber X, the distance r between the satellite S and core C, the differential cross section $d\sigma/d\Omega_i$ of the free X–S collision, and the masses of m_c, m_s, and m_X of the core, satellite, and perturber, respectively. We also describe our numerical verification that this algorithm obtains all allowed trajectories and no false trajectories.

Step 1: Reformulate the scattering problem in terms of a core of infinite mass by calculating the reduced mass μ_s of the satellite–core system from Eq. (14e), the effective mass m_p of the perturber from (14d), and the effective relative speed v_p from (13).

Step 2: Evaluate the initial speed v_α from the conservation of energy equation (23) and the radial component of velocity from (24) to within a sign k. Then calculate the momenta $\rho_\alpha=\mu_s v_\alpha$ and $\rho_p=m_p v_p$, and the angles β from Eqs. (37d) and (37e), and θ_L from Eq. (18).

Step 3: Repeat the following steps for each of the four possible combinations of signs $k=\pm1$ and $k'=\pm1$.

(3a) Evaluate $\Delta\omega$, $\Delta\lambda$, and Δm from Eqs. (31a)–(33).

(3b) For $m=m'=0$, evaluate the coefficients c_i and d_i from Table II; for all other combinations of m and m', calculate a_i and b_i from Table I.

(3c) If $m=m'=0$, find the zeros $\{x_i\}$ of the reaction polynomial $R_{xn}^0(x)$ of Eq. (46b). For all other values of m and m', find the zeros $\{x_i\}$ of $R_{xn}(x)$ defined by Eq. (46a).

(3d) Each zero x_i between -1 and $+1$ corresponds to an allowed trajectory of state-changing collision from an orbit with an initial Runge–Lentz vector defined by ϕ_c, where $\sin\theta_L\sin\phi_c=x_i$. For each x_i, first evaluate $\phi_{c+}=\arcsin[x_i/\sin\theta_L]$ and $\phi_{c-}=\pi-\phi_{c+}$. Then, to determine the allowed trajectories, examine the functions $G_0(\theta_L,\phi_c)$ [Eq. (45f)] for $m=m'=0$ or $G(\theta_L,\phi_c)$ [Eq. (45e)] for any other combination of m and m'. Thus, for $m=m'=0$, if ϕ_{c+} corresponds to an allowed trajectory, then $G_0(\phi_{c+})$ will equal zero. If, however, $G_0(\phi_{c+})$ is nonzero, then $G_0(\phi_{c-})$ will be zero, in which case ϕ_{c+} corresponds to an allowed trajectory. Similarly, for $m\neq0$ and/or $m'\neq0$, if ϕ_{c+} corresponds to an allowed trajectory, then $G(\phi_{c+})$ will be zero. If not, then $G(\phi_{c-})$ will be zero, in which case ϕ_{c+} corresponds to an allowed trajectory. In this manner, determine the values ϕ_{ci} for each $-1\leqslant x_i\leqslant+1$ that causes the function $G(\theta_L,\phi_c)$ to become zero.

(3e) Use Eqs. (36) and (37) to evaluate the matrix A for each value of ϕ_{ci}. Invert this matrix and evaluate the center-of-mass scattering angles θ_i and ϕ_i using Eq. (35).

Step 4: Use Eq. (47) to evaluate the transfer function.

To verify this algorithm, we examined several cases for ''missing trajectories'' and ''false trajectories.'' By a missing trajectory we mean an allowed state-changing trajectory that is not found from the roots of the reaction polynomials. To test for this possibility, we performed a Monte Carlo simulation of scattering events for arbitrary initial conditions and scattering angles. For each event, following steps 1–3 recovered the correct scattering angles θ_i and ϕ_i, verifying that this algorithm identifies all allowed trajectories.

By a false trajectory we mean a set of scattering angles

TABLE II. Coefficients c_i and d_i for the evaluation of $G_0(\theta_L,\phi_c)$ and R_{xn}^0 can be generated by multiplying each table entry by $(r^2\mu_s^2/\hbar^3M^2)$.

i	$c_i(\hbar^3M^2/r^2\mu_s^2)$	$d_i(\hbar^3M^2/r^2\mu_s^2)$
0	$2m_p\,\Delta\omega\,r^2\rho_\alpha^2\,s\beta^2+[(\rho_\alpha\,\Delta\lambda-M\,r\,\Delta\omega\,c\beta)^2$ $+\rho_p^2\Delta\lambda^2+M^2r^2\,\Delta\omega^2\,s\beta^2]\hbar$	$2\Delta\lambda\,\rho_p[\rho_\alpha^2\,r\,s\beta^2$ $+(M\,r\,\Delta\omega-\rho_\alpha\,\Delta\lambda\,c\beta)\hbar]$
1	$2\rho_p\,\rho_\alpha s\beta[\Delta\lambda\,r\,\rho_\alpha\,c\beta+(m_p-\mu_s)r^2\,\Delta\omega+\Delta\lambda^2\hbar]$	$2\Delta\lambda\,\rho_p^2\rho_\alpha r\,s\beta$
2	$2\rho_p^2r(\Delta\lambda\,\rho_\alpha c\beta-\mu_s r\,\Delta\omega)$	

$$M=m_p+\mu_s,\quad c\theta=\cos\theta_L,\quad s\beta=\sin\beta,\quad c\beta=\cos\beta$$

determined from steps 1–3 that does not correspond to an allowed state-changing collision. To test for this possibility, we proceeded as follows. As we evaluated the transfer function $T_{\alpha\alpha'}$ we used the value of ϕ_{ci} from steps 1–3 to find the initial velocity and position of the satellite, $\mathbf{r}_\alpha$ and $\mathbf{v}_\alpha$ [see Eqs. (19a) and (20a)]. We then used the scattering angles θ_i and ϕ_i from step 3(e) to evaluate the final velocity $\mathbf{v}_{\alpha'}$ and position $\mathbf{r}_{\alpha'}$ of the satellite. In all cases, we verified that these quantities did in fact correspond to the quantum numbers n', l', and m', demonstrating that the algorithm does not produce false trajectories.

V. RESULTS FOR CA–HE COLLISIONS

Transfer functions $T_{\alpha,\alpha'}$ for the Ca–He scattering process (1) are shown as a function of the Ca–He velocity v_X and the distance r from the Ca^+ core to the Rydberg electron in Fig. 3. This transition can occur at any of the values of v_X and r shown, but the cross section is dominated by transitions either close to the core or at one or two discrete electron–core distances. It is perhaps not surprising that so severely constrained a scattering process is dominated by a few orbits. More surprising are the spikes that modulate these transition ''ridges.'' These spikes are not those seen in the quantum impulse or time-dependent semiclassical results of Fig. 1; the latter shows only relatively gentle oscillations arising from purely quantum-mechanical interference phenomena.[3]

Convolution of the transfer function with initial and final radial probability functions for the Rydberg electron yields the number differential cross section. This raises the question of whether to use the classical radial distribution $P_\alpha(r) = 2/T|v_{\alpha r}|$ or its quantum-mechanical counterpart in these calculations. The differences between these distribution functions (see Fig. 2 of Ref. 31) suggest that they may yield qualitatively different cross sections.

To completely isolate the effects of quantizing the initial and final energy and the angular momentum from all other quantum-mechanical features, one would use the classical radial distribution. If, however, one seeks a more realistic model—e.g., for comparison to quantal calculations or experimental data—then one may prefer to use the quantum-mechanical radial probability density. In either case, once the transfer function has been calculated, cross sections are easily obtained. Figure 4 compares the number differential cross sections to the quantal results of Isaacs and Morrison[2] for classical and quantum-mechanical radial functions, respectively. For this scattering process, the two sets of cross sections are similar enough that either can be used to qualitatively interpret certain aspects of the quantal results. The small-scale structures and the occasional narrow spikes are both artifices of the classical model.

In Sec. II we noted the relationship between our number differential cross section and the conventional classical cross section, Eq. (8). To clarify this relationship, we have evaluated the right-hand side of this equation using Monte Carlo integration with varying bin sizes Δ. In Fig. 5 we compare these cross sections as a function of Δ for the $m=0\rightarrow m'=0$ transition. As this parameter decreases, the cross sections change dramatically. Apart from the (spurious) spikes in the number differential cross section, the cross section for small bin sizes agrees with the number differential cross section far better than does the result for $\Delta=1$. (As these results were generated with completely different algorithms and computer codes, they also verify that in the limit $\Delta\rightarrow 0$ the classical trajectory and number differential cross sections agree, thereby confirming the latter calculation.) As discussed elsewhere in this paper, the spikes in the cross section for small Δ arise from constraints on the scattering process in our classical model.

Considering the nature of the process we are trying to model, the *quantitative* disagreements between our number differential cross sections and the quantum-mechanical impulse results are not surprising. We consider two features of the comparison in these figures to be significant. First, the overall agreement in magnitude between the classical and quantal cross sections validates using large-scale features of the classical cross sections to qualitatively interpret large-scale features of the quantal results. Second, the clear presence of alignment phenomena in the classical cross sections (the partial magnetic sublevel cross sections for different $|m|$ are not equal) supports an interpretation of these phenomena based on the present classical model.

Although the $m=0\rightarrow m'=0$ cross section exhibits significantly more structure than the other state-to-state cross sections, the difference in transfer functions between the various transitions is less remarkable. The transfer function for each $m\rightarrow m'$ transition is nonzero at the outer classical turning point, but for $m=0\rightarrow m'=0$, particularly strong features appear in this distant region. Because these features correspond to positions where the classical radial probability distribution is infinite and the quantum radial probability is large, they dramatically affect the number differential cross sections.

Although we originally developed this model to study the qualitative dependence of these cross sections on relative velocity, it can also be used to estimate quickly the cross section for a scattering process interest and to determine whether a particular process will be most sensitive to collisions that happen close to or far from the core. We caution, however, against using it for quantitative predictions. To illustrate, we show the total cross section for the $17d\rightarrow 18p$ transition in Fig. 6. While both the quantum and number differential calculations predict *qualitatively* similar dependence on relative speed, the quantum cross section is roughly a factor of 2 stronger and does not display the (spurious) spikes that appear in the classical cross section. Nor does the classical model invariably predict the relative strength of alignment effects at a particular relative velocity, as is evident from the state-to-state cross sections in Fig. 7. Also shown in Fig. 7 is the relative Ca–He velocity distribution for an experiment analogous to those Spain *et al.* performed on Ca–Xe scattering.[14] For such a *gedanken experiment*, the quantal cross sections[2] predict $\sigma^0(v)=37\,a_0^2$, $\sigma^1(v)=67\,a_0^2$, and $\sigma^2(v)=50\,a_0^2$, while the appropriately averaged number differential cross sections are $\sigma^0(v)=45\,a_0^2$, $\sigma^1(v)=29\,a_0^2$, and $\sigma^2(v)=31\,a_0^2$.

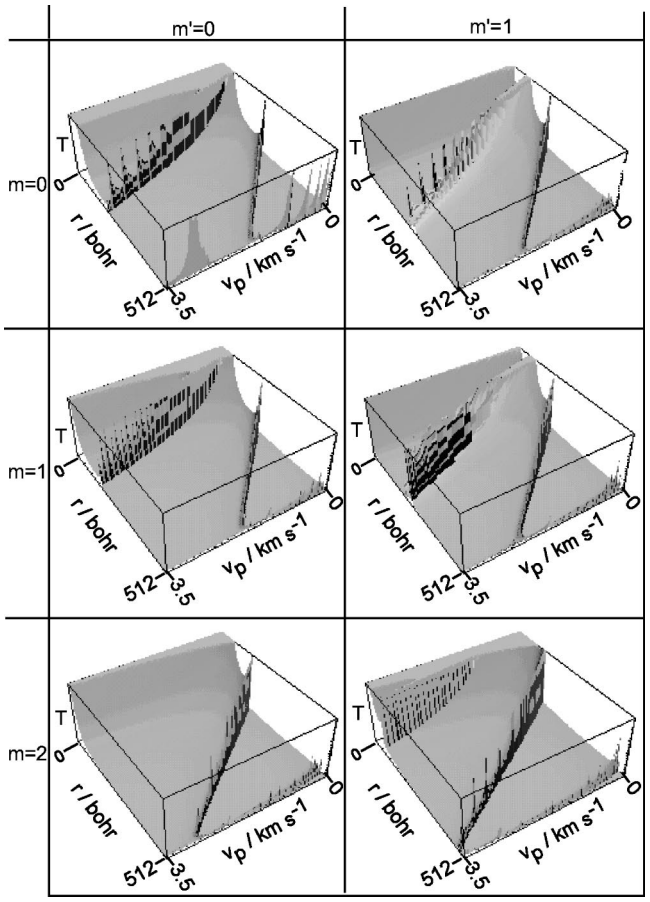

FIG. 3. Surface plots of the transfer function $T_{\alpha,\alpha'}(v_p,r)$ for the $17d \rightarrow 18p$ transition in Ca–He collisions. This function, plotted on the vertical axis, ranges from 0.0 to $1.0\times10^5\ a_0^3$. [The transfer functions for $(n,l,m) \rightarrow (n',l',m')$ are rigorously equal to those for $(n,l,-m) \rightarrow (n',l',-m')$ and are equal to graphical accuracy to those for $(n,l,m) \rightarrow (n',l',-m')$ and for $(n,l,-m) \rightarrow (n',l',m')$. Hence, we do not show these cases.]

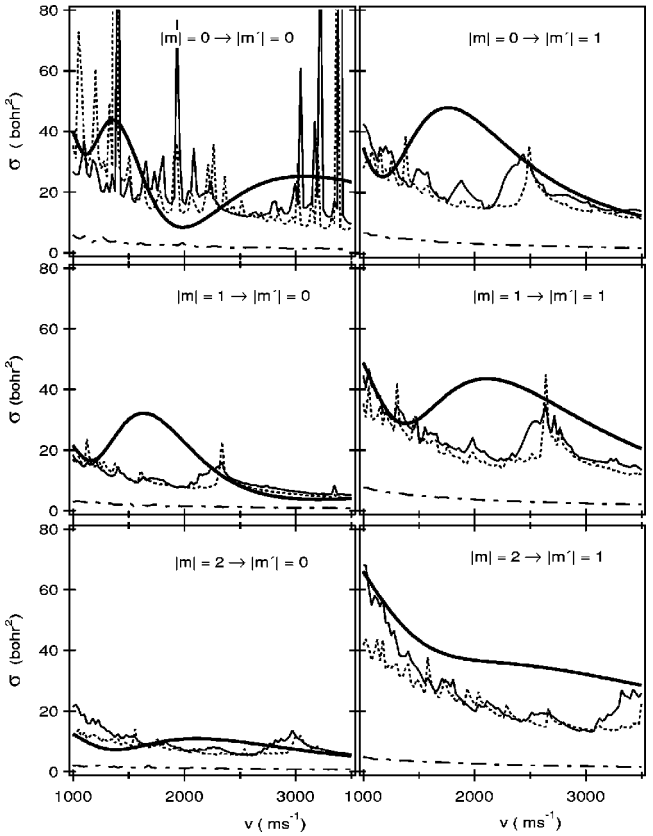

FIG. 4. Comparison of classical and quantum-mechanical state-to-state cross sections for $17d \rightarrow 18p$ transitions in Ca–He scattering. Thin solid line: classical results calculated from the classical radial probability distribution. Dotted line: classical calculations based on the quantum-mechanical radial probability density in the convolution integral of Eq. (3). Thick solid line: quantum-mechanical results of Isaacs and Morrison (Ref. 2). Dashed line: cross sections from a classical trajectory calculation of the right-hand side of Eq. (8) with $\Delta = 1.0$.

VI. CONCLUSIONS

The classical model described in Secs. II and III and schematized in the procedure of Sec. IV yields the number differential cross section defined in Eq. (7) (in the point contact approximation) in terms of the transfer function of Eq. (44). On can use the step-by-step algorithm in Sec. IV to determine this function from the masses of the core, satellite, and perturber, and the differential cross section for elastic scattering of the satellite by the perturber. These calculations, and subsequent evaluation of the number differential cross section, can be performed in short order using MATHEMATICA on a personal computer. (Readers interested in using this algorithm can download a MATHEMATICA notebook and accompanying package from one of the authors' web sites.[36]) One can use the results to estimate the magnitudes of state-to-state cross sections and to quantify the effect of constraining the initial and final state on the distance between the core and satellite during energy transfer.

The transfer functions for the $17d \rightarrow 18p$ transitions in Ca–He scattering reveal discrete regions in phase space that dominate this process. The highly structured dependence of the transfer function on scattering angle leads to considerable small-scale structure (and the occasional spike) in the num-

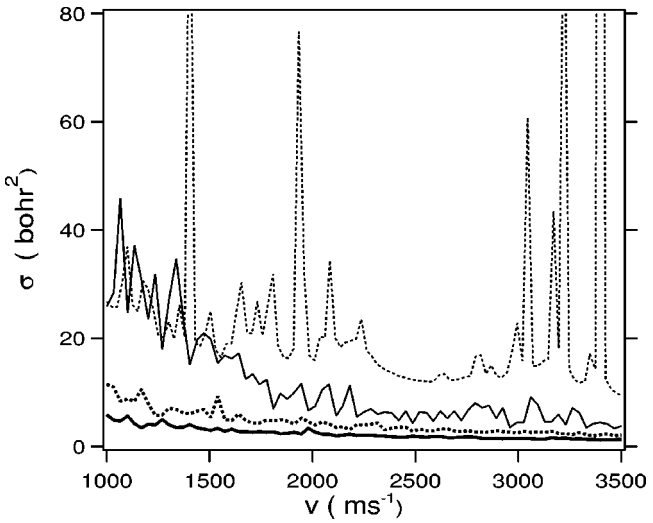

FIG. 5. Classical state-to-state cross sections for the $17d \rightarrow 18p$ transition in Ca–He scattering for $|m| = 0 \rightarrow |m'| = 0$. Light dotted line: the number differential cross section defined by Eq. (7). Also shown are cross sections from an independent, Monte Carlo classical trajectory calculation of the right-hand side of Eq. (8): $\Delta = 1$ (thick solid line), $\Delta = 0.5$ (heavy dotted line), and $\Delta = 0.1$ (regular solid line).

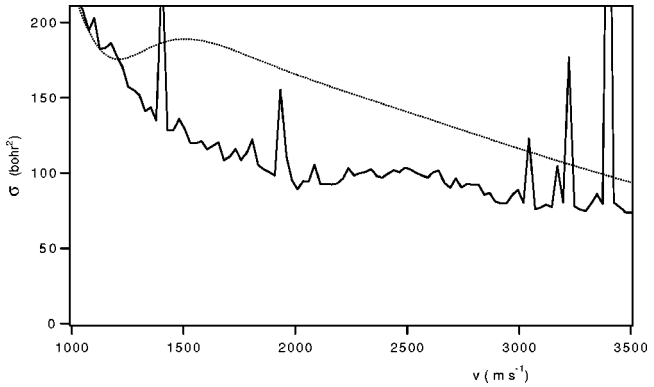

FIG. 6. Total cross sections for $17d \rightarrow 18p$ transitions in Ca–He scattering. Solid line: the classical number differential cross section. Dotted line: the quantum-mechanical results of Isaacs and Morrison (Ref. 2).

ber differential cross sections. These arise purely from postulating quantization of the initial- and final-state energy, angular momentum, and projection of the angular momentum on an axis coincident with the initial relative velocity. We emphasize again that these structures are not those of the quantal cross sections, which arise from quantum-mechanical interference.[3] Nor are they conventional scattering resonances. From the classical point of view, these structures are expected, as a consequence of the sharp oscillations in the state-to-state transition probabilities as a function of the relative collision speed and the core–satellite distance. In a conventional semiclassical treatment such as that of Morrison *et al.*,[3] the uncertainty principle blurs simultaneous specification of the relative speed and distance, smoothing out these structures.

The model results in Sec. V show that alignment phenomena in collisions of rare-gas atoms with aligned Rydberg atoms arises from the constraints imposed on the collision by conservation of energy and angular momentum. In a future publication, we intend to apply the present model to more conventional heavy-particle scattering problems using the model of a harmonically bound rigid rotor using results that appear in this paper.

ACKNOWLEDGMENTS

We acknowledge the support of the Petroleum Research Fund (No. PRF 32187-G6), the National Research Council (No. NRC-6224), and the National Science Foundation (No. PHY–9722055).

APPENDIX: DERIVATION OF THE NUMBER DIFFERENTIAL CROSS SECTION FROM THE BOLTZMANN TRANSPORT EQUATION

We assume without loss of generality that the masses of the cores are much greater than those of any other particles in the system (see Sec. III A). Then, a classical state of the system can be described by the distribution functions $\{F(\mathbf{r}_s,\mathbf{v}_s),G(\mathbf{R}_p,\mathbf{v}_p)\}$, where $F(\mathbf{r}_s,\mathbf{v}_s)$ refers to satellite positions and velocities with respect to the (stationary) core and $G(\mathbf{R}_p,\mathbf{v}_p)$ refers to perturber positions and velocities with respect to the origin of a laboratory-fixed frame. Boltzmann's transport theory then gives the time-dependent evolution of the system due to core–perturber collisions in terms of the coupled set of integral-differential equations

$$\frac{\partial F(\mathbf{r}_s,\mathbf{v}_s')}{\partial t} = -\frac{\partial \mathbf{r}_{s'}}{\partial t}\frac{\partial F(\mathbf{r}_s,\mathbf{v}_s')}{\partial \mathbf{r}_s} - \frac{\partial \mathbf{v}_{s'}}{\partial t}\frac{\partial F(\mathbf{r}_s,\mathbf{v}_s')}{\partial \mathbf{v}_s'} + \int\int u_r\left(\frac{d\sigma}{d\Omega_i}\right)[F(\mathbf{r}_s,\mathbf{v}_s[\mathbf{v}_s',\mathbf{v}_p',\Omega_i]) \times G(\mathbf{R}_p,\mathbf{v}_p[\mathbf{v}_s',\mathbf{v}_p',\Omega_i])] - F(\mathbf{r}_s,\mathbf{v}_s')G(\mathbf{R}_p,\mathbf{v}_p')\}\, d\Omega_i\, d\mathbf{v}_p', \tag{A1a}$$

$$\frac{\partial G(\mathbf{R}_p,\mathbf{v}_p')}{\partial t} = -\frac{\partial \mathbf{R}_p}{\partial t}\frac{\partial G(\mathbf{R}_p,\mathbf{v}_p')}{\partial \mathbf{R}_p'} + \int\int u_r\left(\frac{d\sigma}{d\Omega_i}\right) \times\{F(\mathbf{r}_s,\mathbf{v}_s[\mathbf{v}_s',\mathbf{v}_p',\Omega_i]) \times G(\mathbf{R}_p,\mathbf{v}_p[\mathbf{v}_s',\mathbf{v}_p',\Omega_i])\} - \{F(\mathbf{r}_s,\mathbf{v}_s')G(\mathbf{R}_p,\mathbf{v}_p')\}\, d\Omega_i\, d\mathbf{v}_s'. \tag{A1b}$$

The first two terms on the right-hand side of (A1a) describe the evolution of the classical distribution function $F(\mathbf{r}_s,\mathbf{v}_s')$ as the satellites move in their orbits without undergoing collisions. The integral term is the contribution to the evolution of $F(\mathbf{r}_s,\mathbf{v}_s')$ from satellite–perturber collisions. The vector functions $\mathbf{v}_s[\mathbf{v}_s',\mathbf{v}_p',\Omega_i]$ and $\mathbf{v}_p[\mathbf{v}_s',\mathbf{v}_p',\Omega_i]$ are the initial velocities for a satellite and perturber that scatter through angle Ω_i to produce final velocities $\mathbf{v}_s'$ and $\mathbf{v}_p'$.

In an ideal scattering experiment, we study the formation of the final state a very short time after creation of a well-defined initial state represented by $\{F(\mathbf{r}_s,\mathbf{v}_s),G(\mathbf{R}_p,\mathbf{v}_p)\} = \{f_\alpha(\mathbf{r}_s,\mathbf{v}_s),g_0(\mathbf{R}_p,\mathbf{v}_p)\}$. Because we are interested in experiments in which a very small fraction of the perturbers and satellites collide before a measurement is made, we assume the perturber distribution function is unchanging, i.e.,

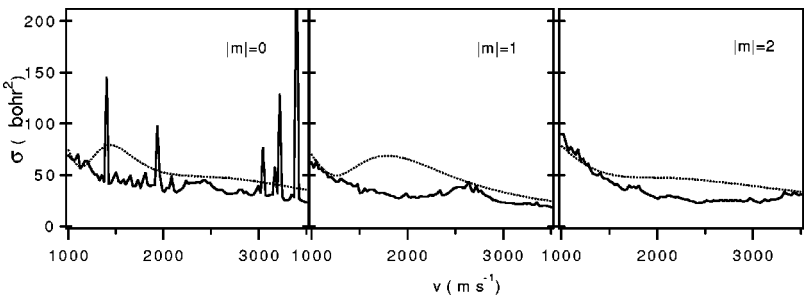

FIG. 7. Partial magnetic sublevel cross sections $\sigma^{|m|}(v)$ for $17d \rightarrow 18p$ transitions in Ca–He scattering. Solid line: cross sections calculated from classical number differential cross sections. Dotted line: quantum-mechanical results of Isaacs and Morrison (Ref. 2). Dashed line: a typical relative velocity distribution for scattering experiments such as those of Ref. 25.

$$G(\mathbf{R}_p,\mathbf{v}_p)=g_0(\mathbf{R}_p,\mathbf{v}_p)=n_p\delta(\mathbf{v}_p-\mathbf{v}_{p,\mathrm{beam}}). \tag{A2}$$

Here, n_p is the number density of perturbers and $\mathbf{v}_{p,\mathrm{beam}}$ is the velocity of an experimentally prepared beam. (The subscript ''beam'' appearing in this Appendix has been suppressed in the body of this paper.) Using this substitution and

$$F(\mathbf{r}_s,\mathbf{v}_s)=f_\alpha(\mathbf{r}_s,\mathbf{v}_s)+f(\mathbf{r}_s,\mathbf{v}_s), \tag{A3}$$

the Boltzmann equation becomes

$$\begin{aligned}\frac{\partial f(\mathbf{r}_s,\mathbf{v}_s')}{\partial t}=&-\frac{\partial \mathbf{r}_s}{\partial t}\frac{\partial f(\mathbf{r}_s,\mathbf{v}_s')}{\partial \mathbf{r}_s}-\frac{\partial \mathbf{v}_{s'}}{\partial t}\frac{\partial f(\mathbf{r}_s,\mathbf{v}_s')}{\partial \mathbf{v}_s'}\\&+\int\int u_r\left(\frac{d\sigma}{d\Omega_i}\right)[f(\mathbf{r}_s,\mathbf{v}_s[\mathbf{v}_s',\mathbf{v}_p',\Omega_i])\\&\times g_0(\mathbf{R}_p,\mathbf{v}_p[\mathbf{v}_s',\mathbf{v}_p',\Omega_i])\\&-f_\alpha(\mathbf{r},\mathbf{v}_s')g_0(\mathbf{R}_p,\mathbf{v}_p')]\,d\Omega_i\,d\mathbf{v}_p'.\end{aligned} \tag{A4}$$

In Eq. (A4) we have assumed that the initial CS state f_α satisfies the steady-state condition

$$\frac{\partial \mathbf{r}_s}{\partial t}\frac{\partial f_\alpha(\mathbf{r}_s,\mathbf{v}_s)}{\partial \mathbf{r}_s}+\frac{\partial \mathbf{v}_s}{\partial t}\frac{\partial f_\alpha(\mathbf{r}_s,\mathbf{v}_s)}{\partial \mathbf{v}_s}=0. \tag{A5}$$

The integral term in Eq. (A4) consists of a positive contribution from collisions that scatter into final state $(\mathbf{r}_s,\mathbf{v}_s')$ and a negative contribution from collisions that scatter from initial state $(\mathbf{r}_s,\mathbf{v}_s')$. Because we are interested in the creation of a new CS state, we evaluate the function f at values of $\mathbf{r}_s$ and $\mathbf{v}_s'$ that correspond to an energy or angular momentum which is different from that of the initial state α. So, we may assume $f_\alpha(\mathbf{r}_s,\mathbf{v}_s')=0$, where

$$\begin{aligned}\frac{\partial f(\mathbf{r}_s,\mathbf{v}_s')}{\partial t}=&-\frac{\partial \mathbf{r}_s}{\partial t}\frac{\partial f(\mathbf{r}_s,\mathbf{v}_s{}')}{\partial \mathbf{r}_s}-\frac{\partial \mathbf{v}_s'}{\partial t}\frac{\partial f(\mathbf{r}_s,\mathbf{v}_s')}{\partial \mathbf{v}_s'}\\&+\int\int u_r\left(\frac{d\sigma}{d\Omega_i}\right)f_\alpha(\mathbf{r}_s,\mathbf{v}_s[\mathbf{v}_s',\mathbf{v}_p',\Omega_i])\\&\times g_0(\mathbf{R}_p,\mathbf{v}_p[\mathbf{v}_s',\mathbf{v}_p',\Omega_i])\,d\Omega_i\,d\mathbf{v}_p'.\end{aligned} \tag{A6}$$

We now introduce delta functions over two new variables of integration, $\mathbf{v}_p$ and $\mathbf{v}_s$, to obtain

$$\begin{aligned}&\frac{\partial f(\mathbf{r}_s,\mathbf{v}_s')}{\partial t}+\frac{\partial \mathbf{r}_s}{\partial t}\frac{\partial f(\mathbf{r}_s,\mathbf{v}_s')}{\partial \mathbf{r}_s}+\frac{\partial \mathbf{v}_s'}{\partial t}\frac{\partial f(\mathbf{r}_s,\mathbf{v}_s')}{\partial \mathbf{v}_s'}\\&=\int\int\int\int u_r\left(\frac{d\sigma}{d\Omega_i}\right)f_\alpha(\mathbf{r}_s,\mathbf{v}_s)g_0(\mathbf{R}_p,\mathbf{v}_p)\\&\quad\times\delta^3(\mathbf{v}_s-\mathbf{v}_s[\mathbf{v}_s',\mathbf{v}_p',\Omega_i])\;\delta^3(\mathbf{v}_p-\mathbf{v}_p[\mathbf{v}_s',\mathbf{v}_p',\Omega_i])\\&\quad\times d\Omega_i\,d\mathbf{v}_p'\,d\mathbf{v}_p\,d\mathbf{v}_s.\end{aligned} \tag{A7}$$

Because the Jacobian of a translation followed by rotation is unity

$$\frac{\partial(\mathbf{v}_s,\mathbf{v}_p)}{\partial(\mathbf{v}_s',\mathbf{v}_p')}=1, \tag{A8}$$

the product of delta functions in Eq. (A7) can be written

$$\begin{aligned}&\delta^3(\mathbf{v}_s-\mathbf{v}_s[\mathbf{v}_s',\mathbf{v}_p',\Omega_i])\;\delta^3(\mathbf{v}_p-\mathbf{v}_p[\mathbf{v}_s',\mathbf{v}_p',\Omega_i])\\&\quad=\delta^3(\mathbf{v}_s'-\mathbf{v}_s'[\mathbf{v}_s,\mathbf{v}_p,\Omega_i])\;\delta^3(\mathbf{v}_p'-\mathbf{v}_p'[\mathbf{v}_s,\mathbf{v}_p,\Omega_i]).\end{aligned} \tag{A9}$$

By substituting Eqs. (A2) and (A9) into the right-hand side of Eq. (A7) and integrating over $\mathbf{v}_p$ and $\mathbf{v}_p'$, one finds the rate $\Gamma(\mathbf{r}_s,\mathbf{v}_s')$ at which satellites are scattered into new orbits with positions $\mathbf{r}_s$ and velocities $\mathbf{v}_s'$, *viz.*

$$\Gamma(\mathbf{r}_s,\mathbf{v}_s')=\frac{\partial f(\mathbf{r}_s,\mathbf{v}_s')}{\partial t}+\frac{\partial \mathbf{r}_s}{\partial t}\frac{\partial f(\mathbf{r}_s,\mathbf{v}_s')}{\partial \mathbf{r}_s}+\frac{\partial \mathbf{v}_s'}{\partial t}\frac{\partial f(\mathbf{r}_s,\mathbf{v}_s')}{\partial \mathbf{v}_s'} \tag{A10a}$$

$$\begin{aligned}&=n_p\int\int\int u_r\left(\frac{d\sigma}{d\Omega_i}\right)f_\alpha(\mathbf{r}_s,\mathbf{v}_s)\\&\quad\times\delta^3(\mathbf{v}_s'-\mathbf{v}_s'[\mathbf{v}_s,\mathbf{v}_{p,\mathrm{beam}},\Omega_i])\,d\Omega_i\,d\mathbf{v}_s.\end{aligned} \tag{A10b}$$

The function $\Gamma(\mathbf{r}_s,\mathbf{v}_s')$ can be convolved with the delta-function probability distribution for a satellite described by $\mathbf{r}_s$ and $\mathbf{v}_s'$ having quantum numbers n', l', and m' to produce the rate at which final states are formed

$$\begin{aligned}\Gamma_{n'l'm'}=&\int\Gamma(\mathbf{r}_s,\mathbf{v}_s')\,\delta(n'-n'[\mathbf{r}_s,\mathbf{v}_s,\mathbf{v}_{p,\mathrm{beam}},\Omega_i])\\&\times\delta(l'-l'[\mathbf{r}_s,\mathbf{v}_s,\mathbf{v}_{p,\mathrm{beam}},\Omega_i])\\&\times\delta(m'-m'[\mathbf{r}_s,\mathbf{v}_s,\mathbf{v}_{p,\mathrm{beam}},\Omega_i])\;d\mathbf{r}_s\,d\mathbf{v}_s'\end{aligned} \tag{A11a}$$

$$\begin{aligned}=&n_pn_{\mathrm{CS}}\int\int\int u_r\left(\frac{d\sigma}{d\Omega_i}\right)P_\alpha(\mathbf{v}_s,\mathbf{r}_s)\\&\times\delta(n'-n'[\mathbf{r}_s,\mathbf{v}_s,\mathbf{v}_{p,\mathrm{beam}},\Omega_i])\\&\times\delta(l'-l'[\mathbf{r}_s,\mathbf{v}_s,\mathbf{v}_{p,\mathrm{beam}},\Omega_i])\\&\times\delta(m'-m'[\mathbf{r}_s,\mathbf{v}_s,\mathbf{v}_{p,\mathrm{beam}},\Omega_i])\,d\Omega_i\,d\mathbf{r}_s\,d\mathbf{v}_s\end{aligned} \tag{A11b}$$

$$=v_p\,n_p\,n_{\mathrm{CS}}\frac{d\sigma_\alpha}{dn'\,dl'\,dm'}. \tag{A11c}$$

In Eq. (A11b) we switched from the distribution function $f_\alpha(\mathbf{r}_s,\mathbf{v}_s)$, which is normalized to the total number of satellites per unit volume, to the classical distribution $P_\alpha(\mathbf{v}_s,\mathbf{r}_s)$, where

$$f_\alpha(\mathbf{r}_s,\mathbf{v}_s)=n_{\mathrm{CS}}P_\alpha(\mathbf{v}_s,\mathbf{r}_s) \tag{A12a}$$

and

$$\int P_\alpha(\mathbf{v}_s,\mathbf{r}_s)\,d\mathbf{r}_s\,d\mathbf{v}_s=1. \tag{A12b}$$

Equation (7) follows immediately from Eq. (A11c).

[1] E. Fermi, Nuovo Cimento **11**, 157 (1934).
[2] W. A. Isaacs and M. A. Morrison, Phys. Rev. A **57**, R9 (1998).
[3] M. A. Morrison, E. G. Layton, and G. A. Parker, Phys. Rev. Lett. **84**, 1415 (2000).
[4] M. O. Hale and S. R. Leone, J. Chem. Phys. **79**, 3352 (1983).
[5] M. O. Hale, I. V. Hertel, and S. R. Leone, Phys. Rev. Lett. **53(24)**, 2296 (1984).
[6] W. Bussert, D. Neuschäfer, and S. R. Leone, J. Chem. Phys. **87**, 3833 (1987).
[7] J. P. J. Driessen and S. R. Leone, J. Phys. Chem. **96**, 6136 (1992).
[8] R. I. Robinson, L. J. Kovalenko, and S. R. Leone, Phys. Rev. Lett. **64**(4), 388 (1990).

[9] E. E. B. Campbell, H. Schmidt, and I. V. Hertel, Adv. Chem. Phys. **72**, 37 (1988).
[10] A. Berengolts, E. I. Dasevskaya, and E. E. Nikitin, J. Phys. B **26**, 3847 (1993).
[11] A. P. Hickman, R. E. Olson, and J. Pascale, in *Rydberg States of Atoms and Molecules*, edited by R. F. Stebbings and F. B. Dunning (Cambridge University Press, Cambridge, England, 1983), Chap. 6, pp. 187–228.
[12] I. L. Beigman and V. S. Lebedev, Phys. Rep. **250**, 95 (1995).
[13] E. M. Spain, M. J. Dalberth, P. D. Kleiber, S. R. Leone, S. S. Op de Beek, and J. P. J. Driessen, J. Chem. Phys. **102**, 9522 (1995).
[14] E. M. Spain, M. J. Dalberth, P. D. Kleiber, S. R. Leone, S. S. Op de Beek and J. P. J. Driessen, J. Chem. Phys. **102**, 9532 (1995).
[15] W. A. Isaacs, Ph.D. thesis, University of Oklahoma (1996).
[16] G. C. Schatz and A. Kuppermann, Phys. Rev. Lett. **35**, 1266 (1975).
[17] F. Webster and J. C. Light, J. Chem. Phys. **85**, 4744 (1986).
[18] F. Webster and J. C. Light, J. Chem. Phys. **90**, 300 (1989).
[19] P. G. Hipes and A. Kuppermann, Chem. Phys. Lett. **133**, 1 (1987).
[20] M. Mladenovic, M. Zhao, D. G. Truhlar, D. W. Schwenke, Y. Sun, and D. J. Kouri, Chem. Phys. Lett. **146**, 358 (1988).
[21] M. Mladenovic, M. Zhao, D. G. Truhlar, D. W. Schwenke, Y. Sun, and D. J. Kouri, J. Phys. Chem. **92**, 7035 (1988).
[22] G. C. Schatz, Annu. Rev. Phys. Chem. **39**, 317 (1988).
[23] J. Z. H. Zhang and W. H. Miller, Chem. Phys. Lett. **153**, 465 (1988).
[24] D. E. Manolopoulos and R. E. Wyatt, Chem. Phys. Lett. **159**, 123 (1989).
[25] J. K. Badenhoop, H. Koizumi, and G. C. Schatz, J. Chem. Phys. **91**, 142 (1989).
[26] T. Peng, D. H. Zhang, J. Z. H. Zhang, and R. Schinke, Chem. Phys. Lett. **248**, 37 (1996).
[27] J. Hare, M. Gross, and P. Goy, Phys. Rev. Lett. **61**, 1938 (1988).
[28] S. B. Hansen, T. Ehrenreich, E. Horsdal-Pedersen, K. B. MacAdam, and L. J. Dubé, Phys. Rev. Lett. **71**, 1522 (1993).
[29] J. C. Day, T. Ehrenreich, S. B. Hansen, E. Horsdal-Pedersen, K. S. Mogensen, and K. Taulbjerg, Phys. Rev. Lett. **72**, 1612 (1994).
[30] K. S. Mogensen, J. C. Day, T. Ehrenreich, E. H. Pedersen, and K. Taulbjerg, Phys. Rev. A **51**, 4038 (1995).
[31] I. Samengo, Phys. Rev. A **58**, 2767 (1998).
[32] C. E. Burkhardt and J. J. Leventhal, Phys. Rev. A **43**, 110 (1991).
[33] V. M. Borodin, A. K. Kazansky, and V. I. Ochkur, J. Phys. B **25**, 445 (1992).
[34] D. Vrinceanu and M. R. Flannery, Phys. Rev. Lett. **82**, 3412 (1999).
[35] T. P. Hezel, C. E. Burkhardt, M. Ciocca, L.-W. He, and J. J. Leventhal, Am. J. Phys. **60**, 329 (1992).
[36] From the URL `www.nhn.ou.edu/~morrison/Research/Papers/`, please navigate to the entry for this paper; there you will find download links for the accompanying MATHEMATICA materials. We welcome feedback from users of these materials and may issue revised versions in response.